

Development of Novel Tapered Pin Fin Geometries for Additive Manufacturing of Compact Heat Exchangers

Julien Cohen¹, David L. Bourell^{1,2}

¹Mechanical Engineering Department

²The Center for Materials Science and Engineering

The University of Texas at Austin

Contact: jhco@utexas.edu

Abstract

Pin fin arrays are widely used to enhance forced convection heat transfer across various industries, finding application in turbine blade trailing edges, electronics cooling, and broadly for compact heat exchange. Fin shape greatly affects flow separation and turbulence generation, and optimizing performance relies on this balance between increased heat transfer and increased pressure loss along the array. Straight circular and elliptical fins are well-characterized in the literature, and there exist a scant few studies on tapered configurations with conventional cross-sections. Recent works have investigated straight pin fins with more complex shapes. Tapered, complex fin geometries represent an avenue for overall performance gains, but manufacturing them is difficult and time-consuming using traditional machining processes. The unique capabilities of additive manufacturing now allow their economical fabrication in an increasing number of fully-dense engineering materials. This work compares 21 pin fin arrays of varying fin cross-section, taper angle, taper profile, and array patterns using experimental and computational methods.

Introduction

Pin fin arrays are widely used to enhance forced convection heat transfer across various industries, finding application in turbine blade trailing edges, electronics heat sinks, compact heat exchangers, and broadly wherever high heat flux removal is required in compact volumes. The use of pin fins increases heat transfer through two main mechanisms: increasing the wetted surface area over which convective heat transfer can occur, and promoting turbulent flow in the inter-fin region of the array [1]–[4]. This turbulence is generated mainly by interrupting boundary layers on the channel walls, and inducing vorticity at the base and in the wake of the fins [5]. Wake flow regimes within these arrays are characterized by complex transitions and strongly three-dimensional flow effects [6].

However, increases in flow obstruction and turbulence are directly related with an increase in pressure loss along the fin array. For many applications where cooling fluid flow is derived from the system itself, specifically in modern gas engine turbine blades used in the aerospace industry, it is desired to minimize this pressure loss to increase overall system efficiency [7]. Even in systems using discrete pumps or fans to provide coolant flow, reducing pressure loss means the system draws less power, is more efficient, and is more environmentally friendly, to produce an equivalent level of heat transfer. Therefore, attaining the highest level of performance from a pin fin array of this type is a nonlinear optimization problem which must holistically balance fin cross-section, taper profile, array spacing, channel geometry, surface

features, and fluid flow characteristics. The history of academic research in this field shows the consistent movement towards higher streamwise aspect ratio, curved, variable profile pin fins.

Conventional circular pin fins are well-characterized in the literature [3], [4], [6], [7]. Tapered pin fins with circular cross-section have received very little public scrutiny, but are investigated in [8], [9]. More recent works have investigated straight pin fins with complex geometries including elliptical [1], [2], [5], [10]–[15], square [5], [16], [17], triangular [5], [6], airfoil derived [5], [13], and teardrop cross-sections [5], [11], [13], [18]. To date, this author has found no example of investigations on tapered pin fins with novel or non-conventional cross-sections.

This work explores the potential performance enhancements of using tapered, complex cross-section pin fin arrays for forced convection heat exchange. Twenty-one array designs, separated into eight geometry families, are investigated using experimental and computation means. Comparisons are made between the members of each geometry family, as well as between families, to illuminate effective means for increasing overall heat exchanger performance. Non-dimensional metrics are defined for heat transfer enhancement, pressure loss, and overall performance to quantitatively compare disparate array configurations. Topics for future work and potential methods for investigation are suggested.

Methodology

Cross-sectional geometries were defined for teardrop shaped pin fins to be used in this work. Each pin consists of a circular section and a tail section defined by two bilaterally symmetric, tangent extensions. Teardrop tail length L and radius R are defined as parameters, as well as a span-wise and stream-wise pitch for the pin pattern, y_n and x_n (Figure 1).

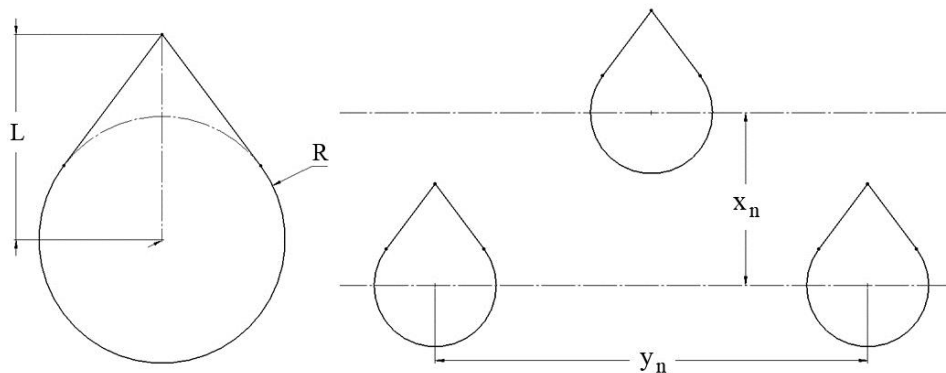


Figure 1: Cross-section of a single pin, and cross-section of three pins within the exchanger pattern.

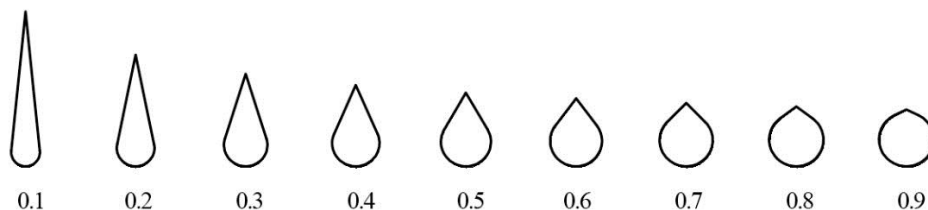


Figure 2: Area normalized teardrop pin geometries with aspect ratios varying from $N = 0.1$ to $N = 0.9$.

An aspect ratio, N , is defined as the ratio of radius and tail length. Using the geometry of the pin, a formula is defined for the radius dependent only on N and the cross-sectional area of the pin, A .

$$N = \frac{R}{L} \quad (1)$$

$$R = \sqrt{\frac{A}{\pi - \cos^{-1} N + \sqrt{N^2 - 1}}} \quad (2)$$

In choosing the form of these equations, it was determined that normalizing by area was of more utility than normalizing by perimeter. The area of each pin more directly correlates with the time and expense required to laser sinter it, as well as the final mass, which is important for performance-driven applications. By holding A constant and defining a set of N values from 0.1 to 0.9, a range of R and L values are calculated. These define the range of potential pin geometries for analysis, shown in Figure 2. The geometry is quantified based on normalization to a circle of radius 3.75 mm.

Three pin geometries were chosen to be tested from this range, to represent the respective extreme ends of the spectrum as well as an intermediate case. 0.2AR, 0.6AR, and 0.8AR are used throughout this work to denote these chosen aspect ratios. Each of the three define a geometry family whose members all have the same initial cross-section at the base of the fin. Five more families are defined for testing, summarized in Table 1 and discussed in the following subsections.

Name	Members	Description
0.2AR	3	High aspect-ratio teardrop shaped fins with a length-radius ratio of 0.2, skinny and long. Straight, low taper, and high taper versions.
0.6AR	3	Medium aspect-ratio teardrop shaped fins with a length-radius ratio of 0.6. Straight, low taper, and high taper versions.
0.8AR	3	Low aspect-ratio teardrop shaped fins with a length-radius ratio of 0.8, short and stubby. Straight, low taper, and high taper versions.
Diameter change	2	Based on the 0.6AR design, these pins decrease in diameter along the streamwise length of the array. Straight and low taper versions.
Nonlinear taper	2	Based on the 0.6AR design, these arrays feature nonlinear tapers along the height of each fin. Convex and concave versions.
SEF	3	The fins on these arrays are Standard Elliptical Fins (SEF), in a straight, low taper, and high taper version.
Swept back		Based on the 0.6AR design, these fins are swept backwards along the height of each fin. Straight and high taper versions.
Triple row	2	Based on the 0.6AR design, these use a pattern which repeats every three rows, rather than every two. Straight and high taper versions.

Table 1: Summary of tested geometry families.

Four of these families are based on the 0.6AR geometry, with novel design features varying the fin shape along the vertical or streamwise axis. The fifth family is based on the Standard Elliptical Fin (SEF), which previous work has shown is more efficient than circular fins in a non-tapered configuration [1], [13], [14]. Each family contains members with varying tapers applied to the fin extrusion, defined by a draft angle relative to the vertical axis. “Straight” members have no taper, effectively a draft angle of 0° . “Low Taper” members have a draft angle of $2\text{-}3^\circ$, and “High Taper” members have a draft angle of $4\text{-}5^\circ$, dependent on geometry limitations. Each fin array is patterned with pitches of $x_n = 10\text{ mm}$ and $y_n = 20\text{ mm}$, with 10.8 mm of flow bypass on each side of the array and 30 mm tall fins. The base of the arrays is $6 \times 4 \times 0.1\text{ in.}$ Every array pattern repeats every two rows with an offset of 10 mm between, except for the two triple repeating designs, which repeat every three rows with an offset of 6.67 mm .

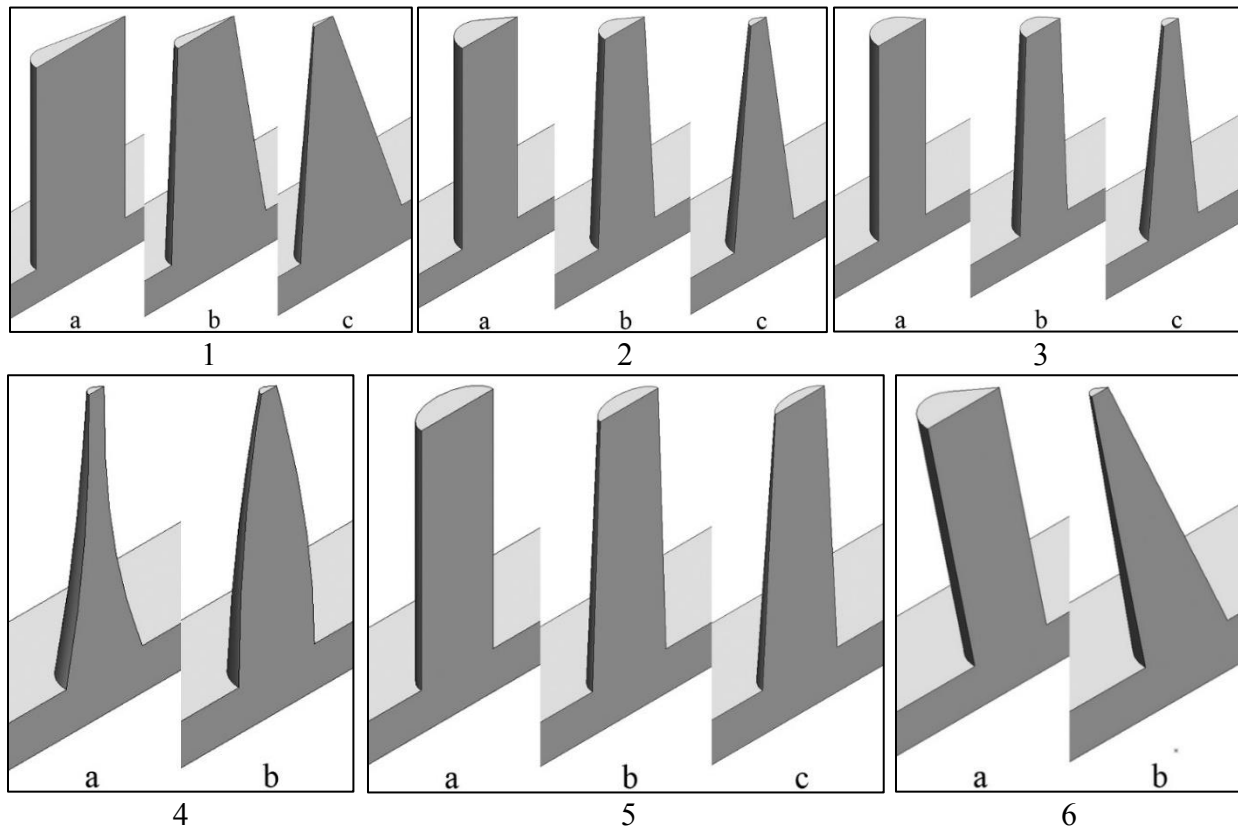


Figure 3: 1: 0.2AR individual fin cross sections: (a) straight, (b) low taper, (c) high taper. 2: 0.6AR individual fin details: (a) straight, (b) low taper, (c) high taper. 3: 0.8AR individual fin details: (a) straight, (b) low taper, (c) high taper. 4: Nonlinear tapered fin array geometries: (a) concave, (b) convex. 5: SEF individual fin details: (a) straight, (b) low taper, (c) high taper. 6: Swept back individual fin details: (a) straight, (b) high taper.

Experimental Testing

Each of the pin fin arrays were fabricated using Nylon 12 PA powder supplied by Stratasys Direct Manufacturing [19] in a 3D Systems Sinterstation HiQ+HS machine. The powder stock was a mixture of fresh powder, overflow, and part cake, at approximately a 30/40/20 percent mass ratio.

A prototype wind tunnel system was created for testing the real-world pressure drop over the various pin fin arrays. This system was designed for a modular, open-loop configuration utilizing a centrifugal blower fan to produce inlet fluid flow with Reynold's number $0-10^4$, allowing drop-in testing of any fin array within the size limitations. Two differential pressure transducers were configured to measure fluid velocity using a pitot-static probe upstream of the test section, and pressure drop over the test section using pressure ports. Data from these transducers were fed through a USB data acquisition (DAQ) module into purpose built Labview software for real-time test monitoring and data logging. Figure 4 shows an overview of the wind tunnel system architecture.

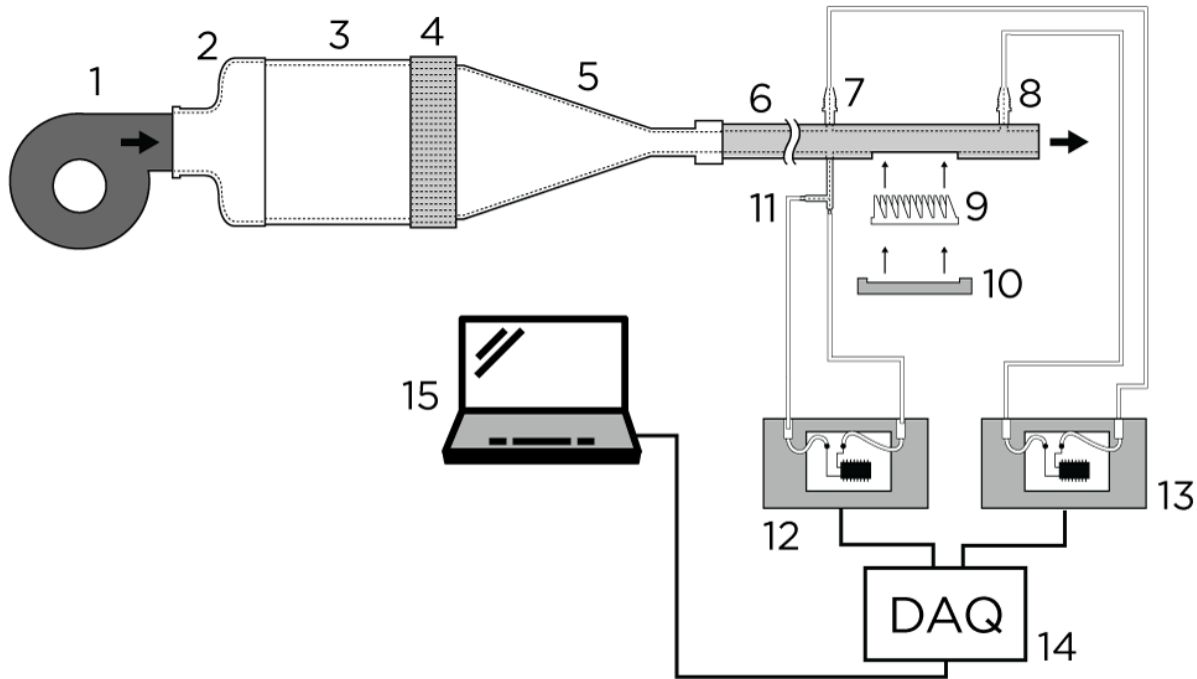


Figure 4: Diagram of wind tunnel system architecture.

A Dayton model 3HMJ1 centrifugal blower (1) uses a squirrel cage rotor to draw in air and accelerate it through the system. The air travels through an expansion section (2) into the settling chamber (3), which allows large-scale turbulent fluctuations to decay [20]. The air passes through a honeycomb filter (4) which aligns the flow parallel to the test section and minimizes lateral variations in the mean and fluctuating velocity [21]. The air then flows through a contraction section (5) into the test section (6), where it interacts with the fin array (9), secured with an airtight seal by the array housing (10). This seal is effected by two rubber gasket strips and clamping pressure. A United Sensor Corp PAD-6-KL pitot-static probe (11) outputs differential pressure to pressure Transducer A (12) to measure fluid velocity, and two pressure ports (7,8) output total pressure to pressure Transducer B (13) upstream and downstream of the fin array to measure pressure drop. Both are Omega PX-277 differential pressure transducers, outputting analog data through a NI USB-6002 data acquisition module (14) to a Labview program running real-time data collection and monitoring (15).

Computational Testing

Simulations were run in ANSYS Workbench 15.0.7 using the FLUENT to handle three-dimensional CFD calculations. Fins were defined as aluminum with a constant temperature input at the bottom surface of the array, using array geometry and fluid flow characteristics equal to the experimental trials. A comparison of the experimental and simulated pressure drop results serves as validation for the accuracy of the simulated fluid flow, as well as a confidence measure for the simulated heat transfer results.

Meshes were created using the ANSYS Meshing module. To minimize the necessary computation resources and time, models were sliced in half bilaterally and symmetry conditions used along the sliced surface. Automatically generated unstructured grids were used to satisfy the complexity of closed-channel fluid flow through an array of obstructions. The meshes were refined around critical areas of low cross-section, such as between pins, and at areas of high aspect ratio, such as at the angled tip of some fins. Inflation layers were utilized to better capture the convective heat transfer effects of turbulent fluid flow near the pin surface, as well as to increase the resolution of internal conductive heat transfer in the pin itself (Figure 5). Initial experiments were performed to determine the necessary mesh resolution for grid-independence, which was defined as a less than 2% difference in overall heat transfer rate between trials. Meshes used in this work utilize 300,000 – 1,000,000 computational nodes depending on array complexity.

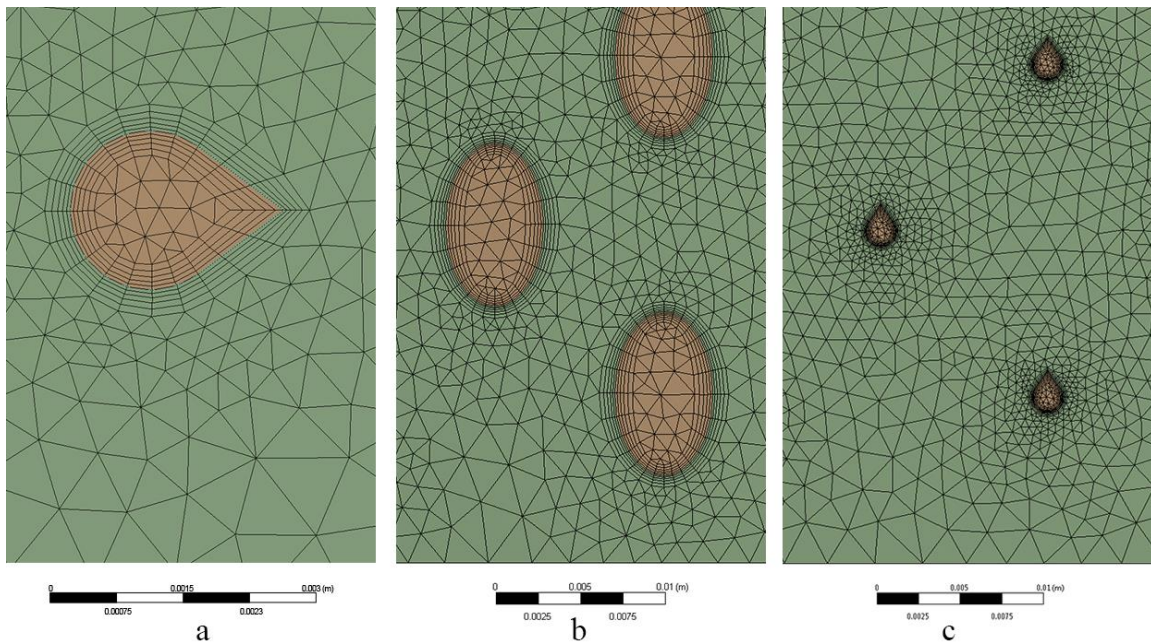


Figure 5: Top-view of meshing detail, illustrating the variable unstructured grid design and inflation layer application. (a) straight 0.6AR fin, (b) low-taper SEF, (c) high-taper 0.6AR.

Solutions were calculated using two linked models. The energy equation was solved for conductive heat transfer within the solid fin array, and convective heat transfer between the fins and the fluid. The standard $k-\epsilon$ turbulence model was applied to calculate fluid flow characteristics, using second-order upwind spatial discretization for pressure, momentum, turbulent kinetic energy, turbulent dissipation rate, and energy parameters. While the first-order algorithms result in faster convergence, second-order is more accurate in cases where flow is not aligned with the grid [22, p. 1409], as it is here with an unstructured grid and obstructed flow.

The SIMPLE pressure-velocity coupling scheme was used, and the gradient discretization was least squares cell based.

Experimental Analysis

Experimental testing produced 10^4 pairs of differential pressure data points per trial, ten trials per fin array, for 21 different fin array geometries. The following process was applied to each data set.

First, the set of analog voltage data points V_{in} were converted to pressure P_{in} using the respective full scale pressure of each transducer P_{FS} . Assuming steady incompressible flow, the resulting pressure from the pitot-static probe is converted to velocity v_{p-s} using air density ρ at environmental temperature and pressure [23].

$$P_{in} = \frac{V_{in}}{10} P_{FS} \quad (1)$$

$$v_{p-s} = \frac{2P_{in,p-s}}{\rho} \quad (2)$$

The standard deviation σ of each data set was calculated, and then an average taken to condense the 10 seconds worth of data into a single value. The error for each data point was calculated using the root-mean-square of the standard deviation and listed 1% full-scale error of the transducers.

$$Error = \sqrt{\sigma^2 + 0.01P_{FS}} \quad (3)$$

The hydraulic diameter of the inlet is calculated using the height, a , and width, b , of the test section aluminum tubing. This was used along with inlet velocity and kinematic viscosity ν to calculate the Reynold's number Re of the flow entering the test section.

$$D_{h,in} = \frac{2ab}{(a+b)} \quad (4)$$

$$Re = \frac{D_{h,in}v_{p-s}}{\nu} \quad (5)$$

Simulation Analysis

Each fin array was simulated individually with inlet fluid velocities of 1, 5, 9.5, and 14 m/s. Each simulation was configured to output a text file with total convective heat transfer rate Q , inlet fluid velocity v_{in} , inlet pressure P_{in} , outlet pressure P_{out} , volume-weighted average temperature of the fluid volume T_{fluid} , and the area-weighted average wall temperature of the heat transfer surface T_{wall} .

First, the hydraulic diameter of the test section $D_{h,test}$ was found using the internal fluid volume V_{fluid} and wetted surface area A_{fluid} . Pressure drop over the array ΔP was found using the difference between inlet pressure P_{in} and outlet pressure P_{out} .

$$D_{h,test} = \frac{4V_{fluid}}{A_{fluid}} \quad (6)$$

$$\Delta P = P_{in} - P_{out} \quad (7)$$

Heat flux q was calculated from the total convective heat transfer rate and transfer area A_{wall} , and was used to find the average convective heat transfer coefficient h_{avg} . This required the average pinwall temperature and average fluid volume temperature.

$$q = \frac{Q}{A_{wall}} \quad (8)$$

$$h_{avg} = \frac{q}{T_{wall} - T_{fluid}} \quad (9)$$

The average Nusselt number Nu was then found using the thermal conductivity k . This is a ratio of convective to conductive heat transfer across the solid-fluid boundary, and an indirect measure of average turbulence in the flow field. Higher values are desired for effective heat exchanger performance. The total pressure loss or friction coefficient f was calculated using the constant air density ρ and inlet velocity. This is a measure of relative pressure loss with respect to inlet flow conditions.

$$Nu_{avg} = \frac{h_{avg} D_{h,test}}{k} \quad (9)$$

$$f = \frac{2\Delta P}{\rho v_{in}^2} \quad (10)$$

Finally, the specific friction loss ϵ_f is calculated as a ratio of the average friction coefficient and average Nusselt number [11], [13]. This is an overall performance index, which indicates the pressure loss required to achieve an equal amount of heat transfer capability through the fin array. Minimizing this parameter equates to a more efficient and effective heat exchanger.

$$\epsilon_f = \frac{f}{Nu_{avg}} \quad (11)$$

Results

Comparison of Experimental and Simulated Pressure Drop Results

Figures 6-7 display a comparison of pressure drop between experimental results and simulated results for each fin array, grouped by geometry family. It is observed that the simulated results increasingly diverge from the experimental results as Reynold's number

increases. This is a result of the simulations, by the design and density of the mesh, and the second-order upwind governing $k-\epsilon$ equations, not capturing the full chaotic behavior of fluid flow in highly turbulent regions within the array [24].

In all cases the experimental pressure drop was greater than the simulated values. One of the major contributors to this disparity was likely the simulated effects of fluid heating on viscosity and turbulence generation. From $Re = 0 - 20,000$ the data sets are highly similar, with mismatch error between 0–12%. In the more turbulent regime between $Re = 20,000 - 50,000$, higher mismatch errors are observed over a broader range, between 5–30%. While less significant error may be required for design purposes, the quantitative correlation and relative similarity between experimental and simulated data sets in this work provide a strong basis for confidence in the validity of the simulated fluid flow characteristics.

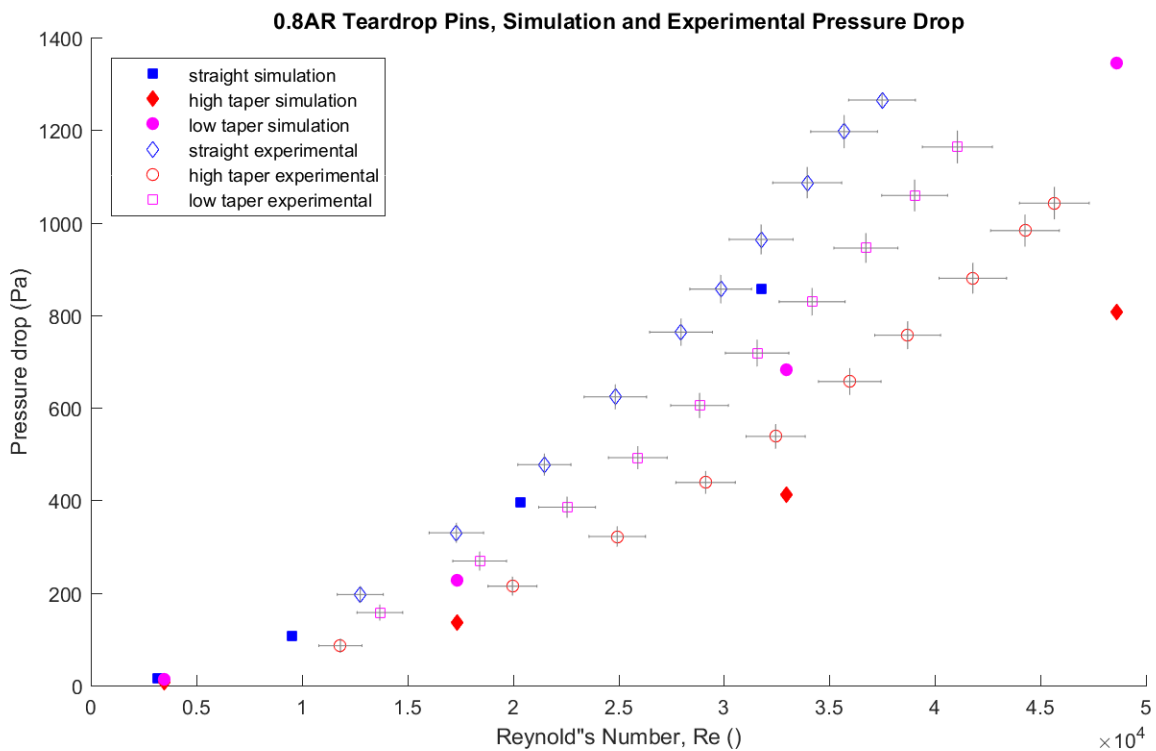


Figure 6: Comparison of experimental and simulated pressure drop across the 0.8AR geometry family.

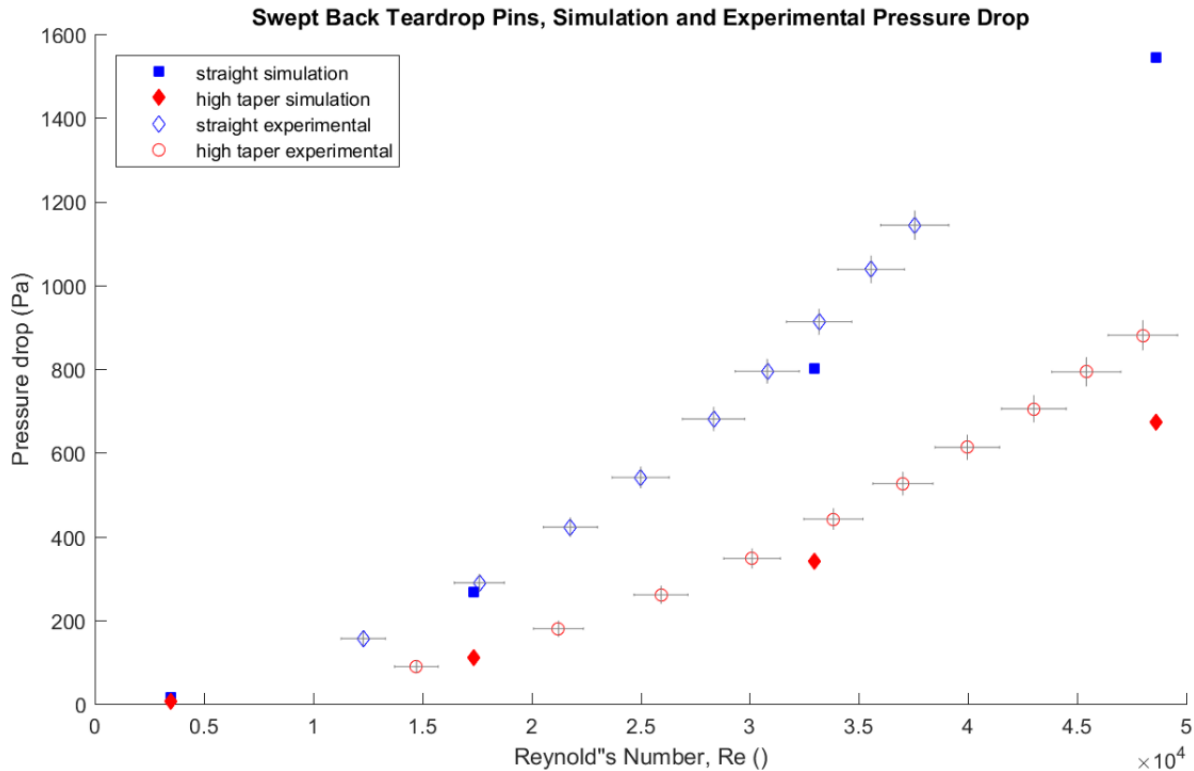


Figure 7: Comparison of experimental and simulated pressure drop across the swept back geometry family.

Simulation Results

Heat Transfer

Figure 8 shows the Nusselt number data sets for each geometry family as well as the circular test case. This metric not a direct measure of heat transfer, but of heat transfer enhancement due to the fins. A best fit line compiled by Ciha from a survey of ten studies on similar fin geometries [25] is presented along with the results of this work, on a log-log scale for direct comparison.

The density of information makes it difficult to glean useful associations between test cases from this plot, but it does serve as an effective comparison between this work and previous works in the literature. 19 of the 21 fin arrays tested align well with this survey data, while the 0.6AR straight and 0.8AR straight arrays are outliers.

Contrasting these two with the circular fin array, which presents less effective heat transfer than the best fit line, the cause of this disparity was a combination of three effects: the high level of flow obstruction in the straight configuration, an increase in length travelled along the fin before flow separation commensurate with the length of the tail, and more efficient heat transport from the base to the fin tip related to cross-sectional radially symmetry. The 0.6AR straight array creates more efficient flow separation but less efficient conductive heat transport, while the 0.8AR straight array creates the opposite effects.

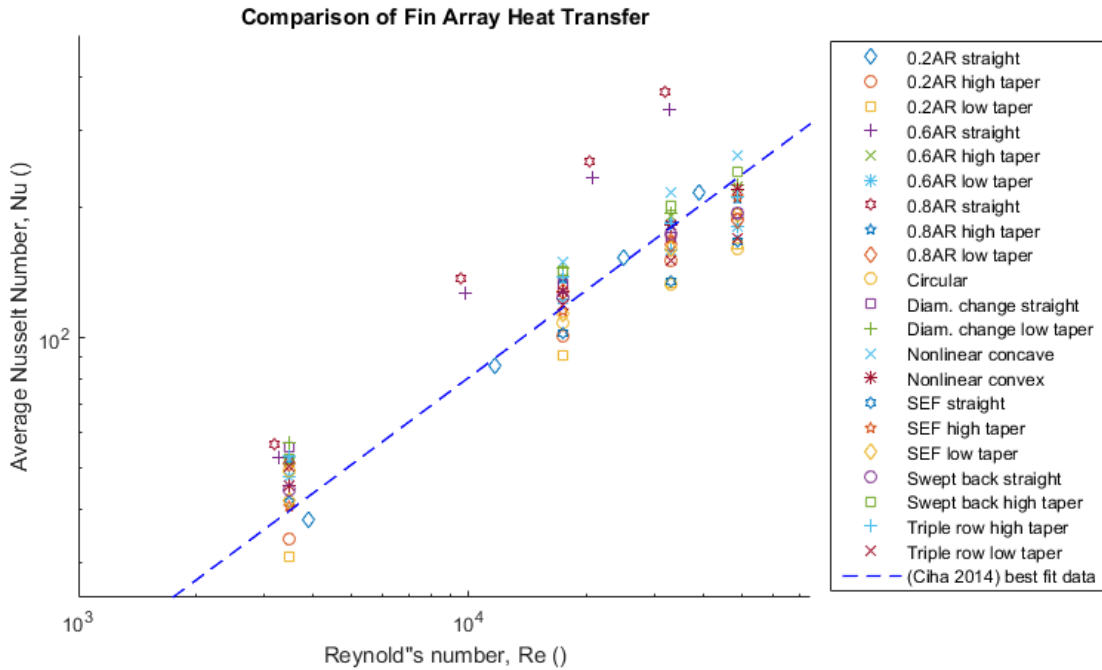


Figure 8: Comparison of average Nusselt number data for all fin arrays. The best fit line is reported from a survey similar pin fin arrays and flow regimes [25].

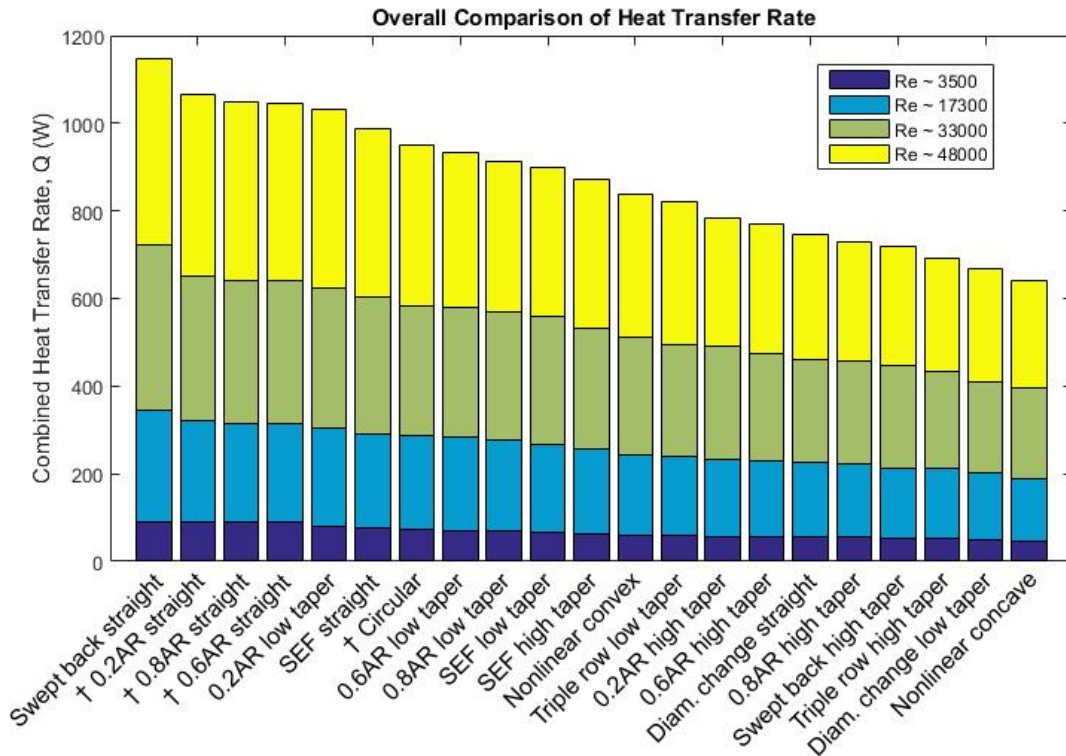


Figure 9: Overall comparison of array heat transfer capacity using the sum of heat transfer rates at four Re inputs, from best to worst. † Values calculated from the best fit equation rather than directly from simulation data.

Figure 9 shows average heat transfer rate for each fin array, area-weighted over the full heat transfer surface in each simulation case, combining sets of data at four inlet flow velocities. These data are presented without normalization to any geometry or fluid parameter, and represent the total amount of energy flowing from the pins to the fluid through convective heat transfer. While the Nusselt number is an effective metric for overall efficiency of heat exchanger arrays, Q represents a pure energy transfer basis for comparison. If pressure drop is not a limiting factor in design, this represents the performance scale for the tested fin arrays. Moving from best to worst constitutes moving through the straight arrays, to the low taper arrays, and finally to the high taper arrays.

Heat transfer results follow the theoretical geometry correlations in these data expected from previous work [6], [11], [13], [18], [26]. Higher flow obstruction induces more turbulent flow and accelerates the fluid through narrower inter-fin channels, and longer fins tails delay flow separation. These phenomena are illustrated in Figures 10-11, which show triptych contour plots of the 0.2AR, 0.6AR, and 0.8AR fin arrays for velocity and turbulent kinetic energy, respectively, on normalized scales.

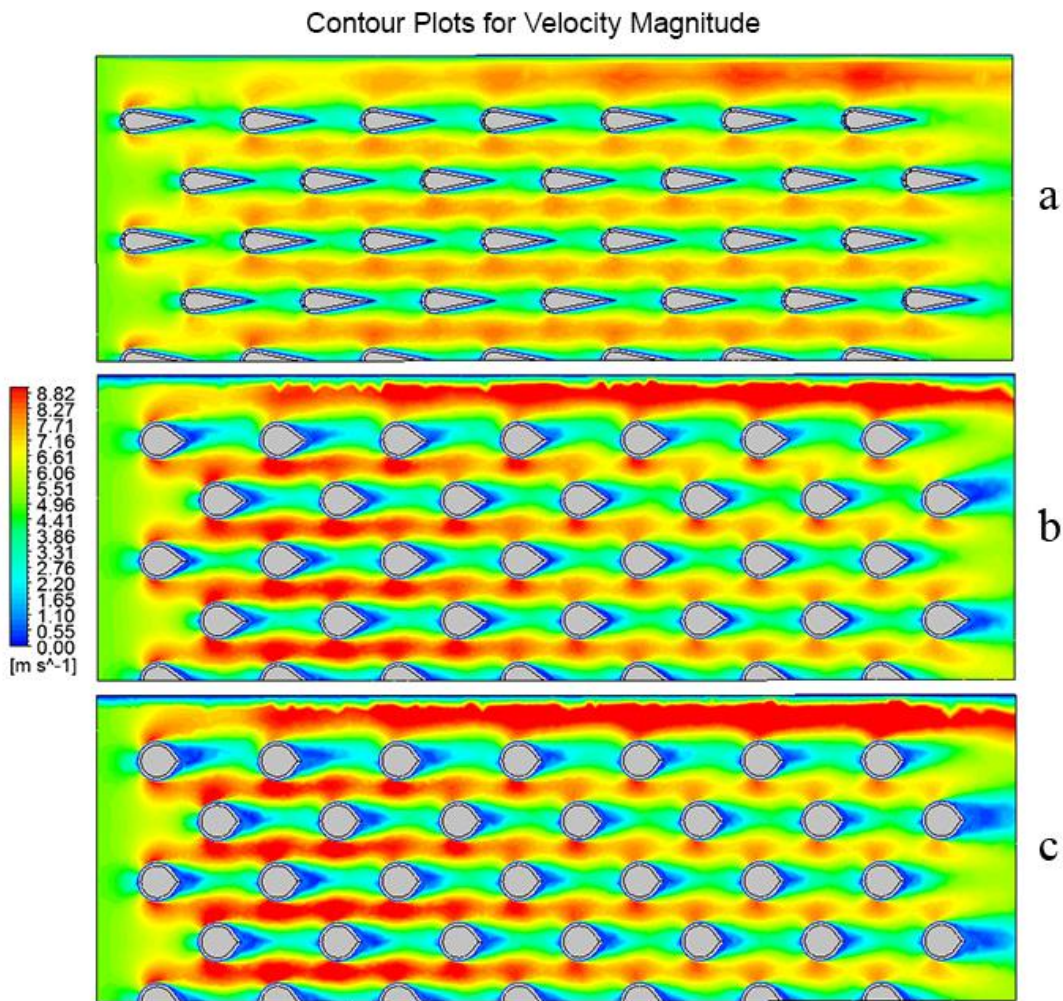


Figure 10: Normalized velocity contour plots of the fluid volume, taken on the horizontal midplane of each fin array. a) 0.2AR, b) 0.6AR, c) 0.8AR.

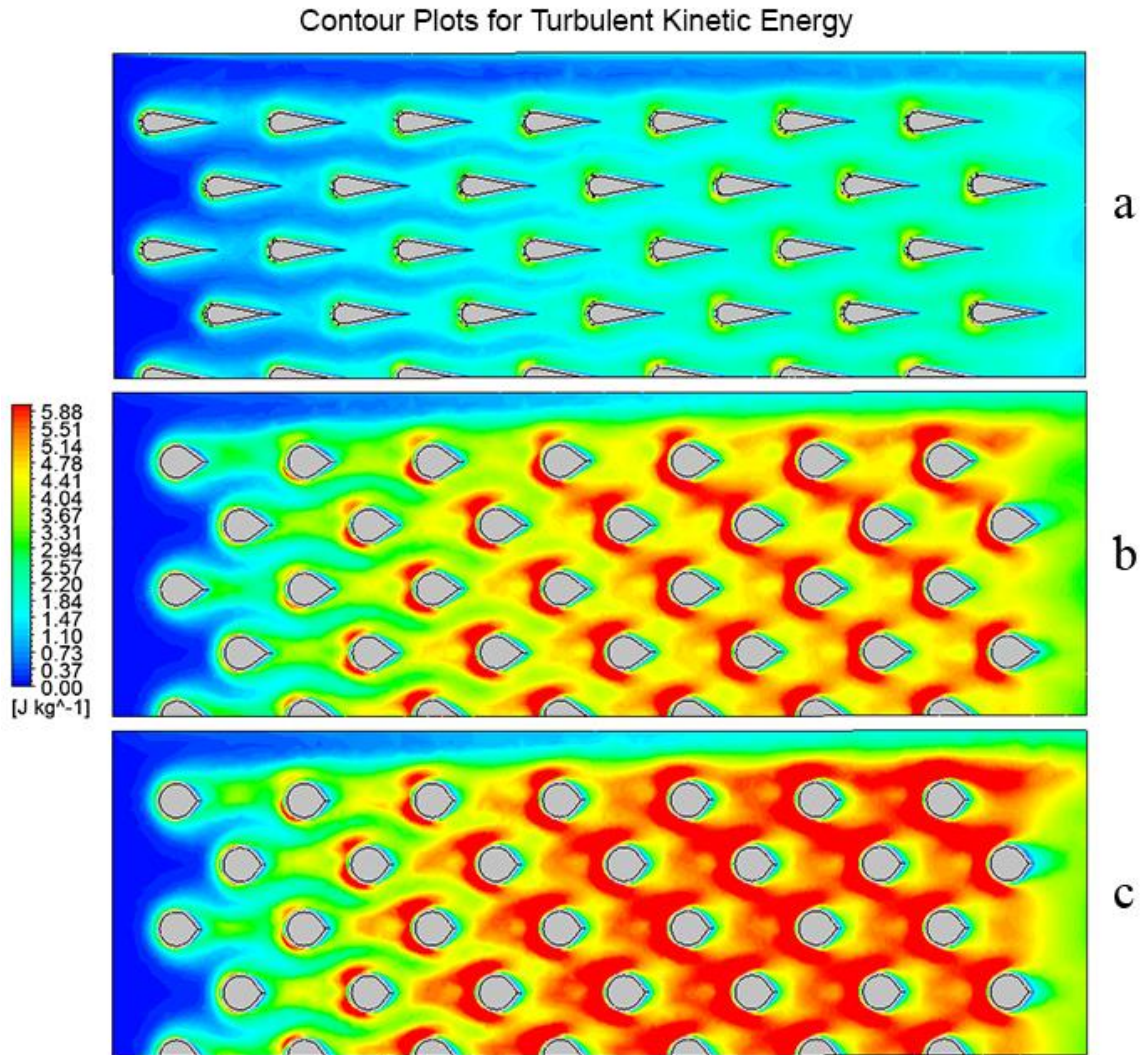


Figure 11: Normalized turbulence contour plots of the fluid volume, taken on the horizontal midplane of each fin array. a) 0.2AR, b) 0.6AR, c) 0.8AR.

Pressure Loss

Figure 12 shows the combined friction coefficient data set for each fin array at four inlet flow velocities, providing a holistic measure of the pressure drop on a geometry basis. The expected trends are evident here for the same fluid-based reasons as in the previous section, but working in reverse: arrays with higher tapers and larger areas of flow bypass exhibit less flow obstruction over the test section, and subsequently a lower overall pressure drop.

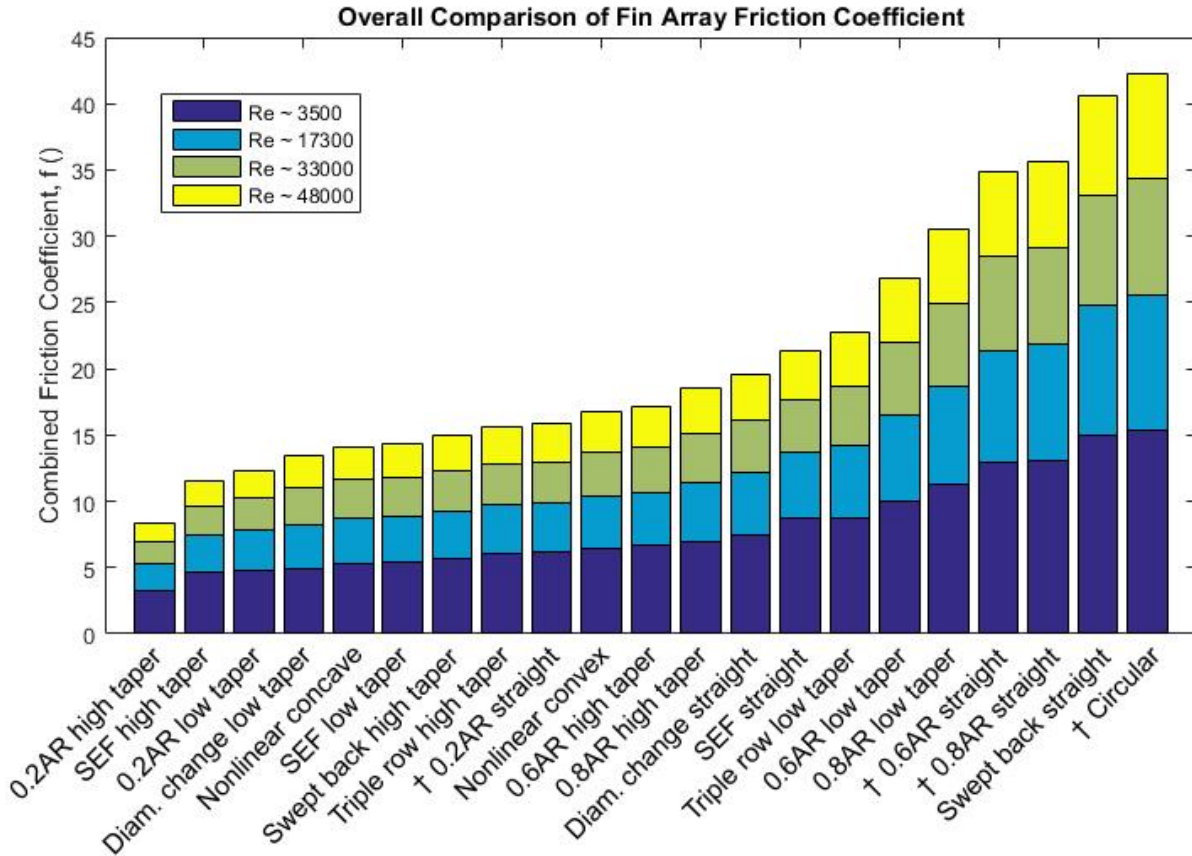


Figure 12: Overall comparison of pressure loss using the sum of friction coefficients at four Re inputs, from best to worst. † Values calculated from the best fit equation rather than directly from simulation data.

Overall Performance

In the previous two sections, some physical mechanisms responsible for the relative differences in heat transfer and pressure drop among the tested fin arrays were discussed. Since these mechanisms affect both parameters in opposite ways, balancing the two becomes a design optimization problem based on fin geometry and array configuration. To quantitatively contrast fin arrays, the non-dimensional specific friction loss metric was introduced in [9]. This is the ratio of friction coefficient to Nusselt number, basically a measure of the pressure loss required to achieve a certain amount of heat transfer capability across the fin array, where lower values are desired. Figure 13 displays an overall comparison of the specific friction loss for each fin array, combining sets of data at four inlet flow velocities. This provides a holistic basis for inter-array comparison. It can be seen that the 0.2AR high taper array is the most effective of those tested in the present work, and furthermore that every design was more effective than the standard circular fin geometry.

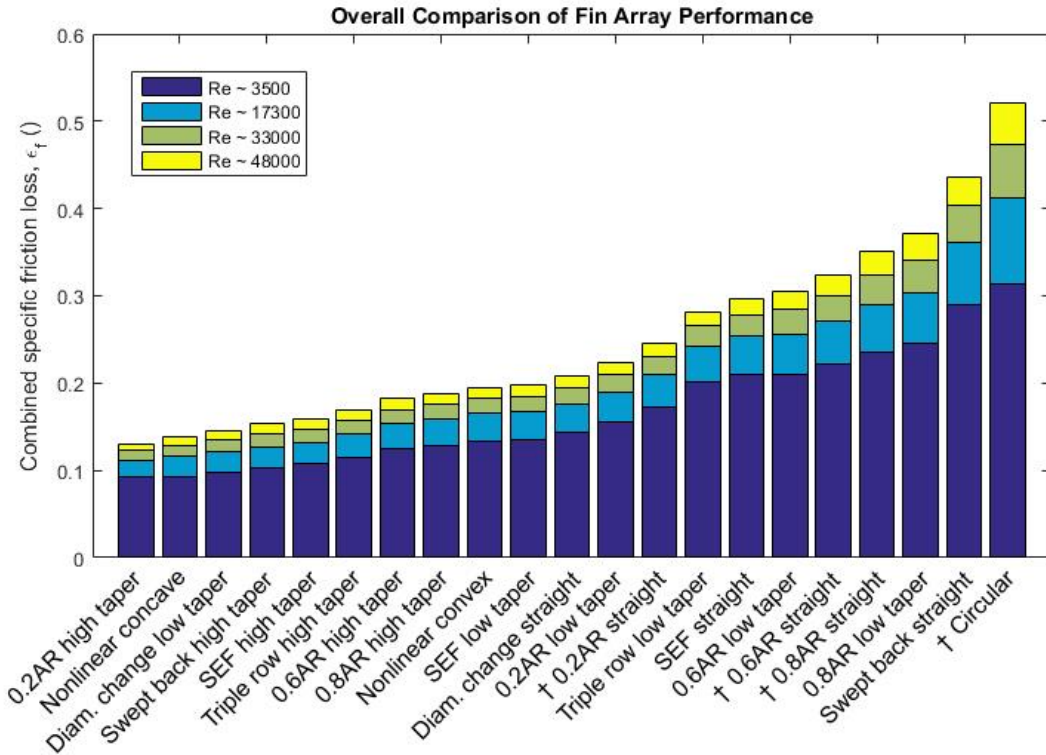


Figure 13: Comparison of array performance using the sum of specific friction loss at four Re inputs, from best to worst. † Values calculated from the best fit equation rather than directly from simulation data.

Discussion

Effect of Tapering on Performance

It is clear from the results of this work that, within each geometry family, increased taper angle correlates with more effective performance. Figure 14 displays this trend in the SEF geometry family, and the causal physical phenomena as described in previous sections are visible in Figures 10-11.

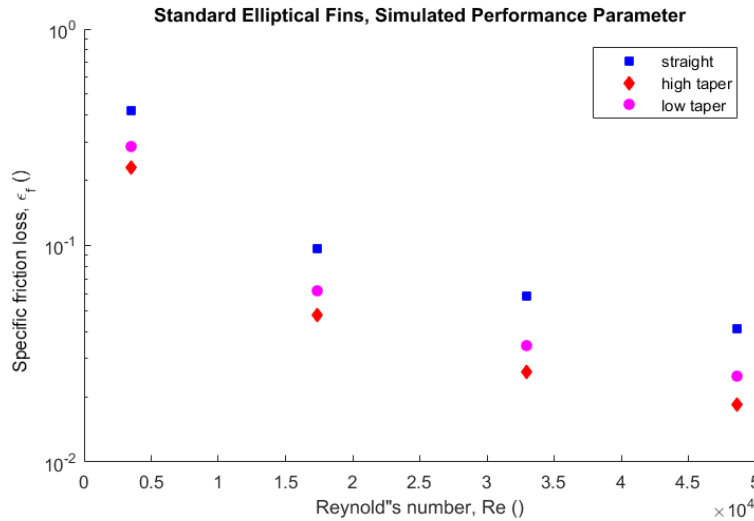


Figure 14: Overall performance of the SEF geometry family, characterized by specific friction loss.

Effect of Varying Fin Dimensions Along the Streamwise Axis

This work represents a proof of concept for diameter changing fins along the length of a heat exchanger array. By varying the cross-sectional geometry of each fin as a function of its location in the fluid stream, both heat transfer efficiency and pressure drop are manipulated, and it was theorized that a favorable ratio of change in these parameters could increase overall performance of the array. This theory has been preliminarily confirmed in this work, as results for the diameter change low taper array place it as the third best performing of the 21 tested (Figure 13).

Figure 15 shows normalized turbulence contour plots for the straight and low taper diameter change arrays. It is observed that turbulence increases as it enters the fin array, reaches a maximum around the fifth row, and then steadily decreases. To increase the effectiveness of these geometries, turbulence should be generated in the initial rows and then maintained, and these results indicate the use of an over-aggressive diameter reduction scheme.

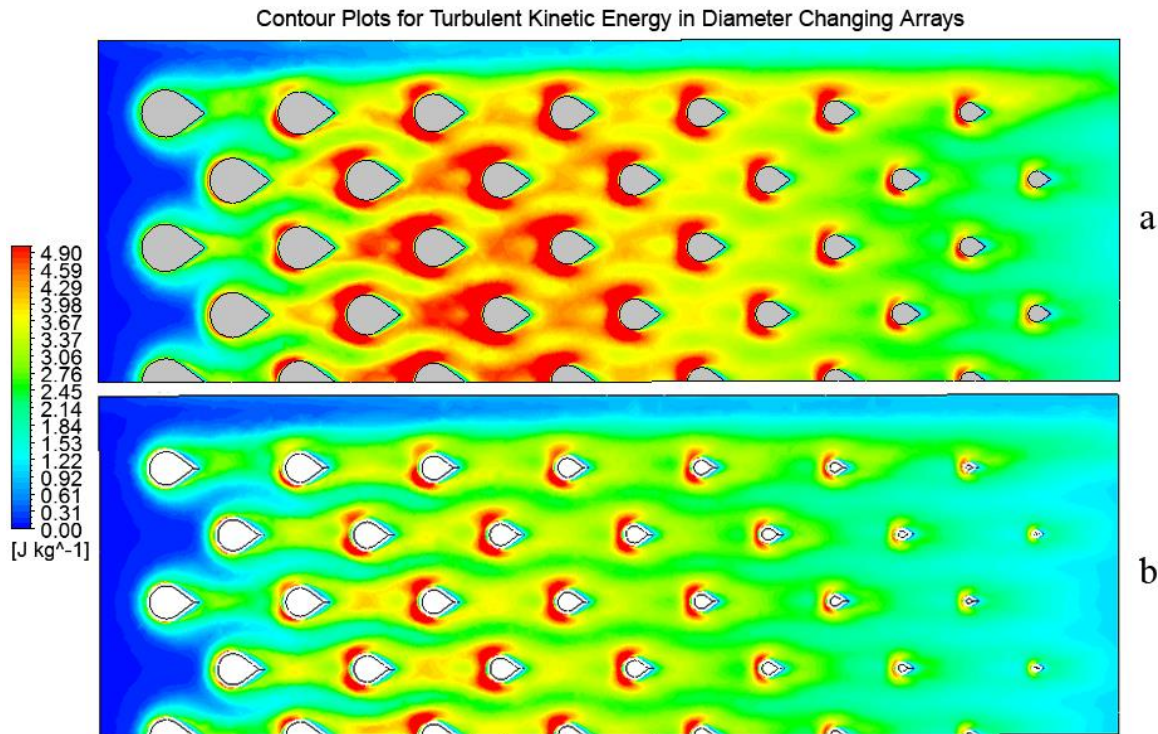


Figure 15: Normalized turbulence contour plots of the fluid volume, taken on the horizontal midplane of each fin array. a) Diameter change straight, b) Diameter change low taper.

Comparison of Linear and Nonlinear Tapers

The comparisons so far made all been used linear tapers, with a constant draft angle between the base and tip of the fin. Considering that the increased performance observed in tapered fins is derived from a greater match between the vertical cross-sectional profile and temperature gradient, and that this gradient is likely nonlinear due to geometry and boundary layer effects at the base, a nonlinear taper has been theorized to effect a higher overall performance in this type of pin fin array [27]. Two nonlinear profiles were tested in this work as a proof of concept for future investigation, both concave and convex. Figure 16 shows the performance of these two arrays compared with the linear tapered version, on a log-log scale with best fit lines shown. It is observed that the convex geometry performance is at best equal to the linear version, with a significant decrease at lower Reynold's number flow. The concave geometry performance is significantly greater than the linear version at all tested flow regimes.

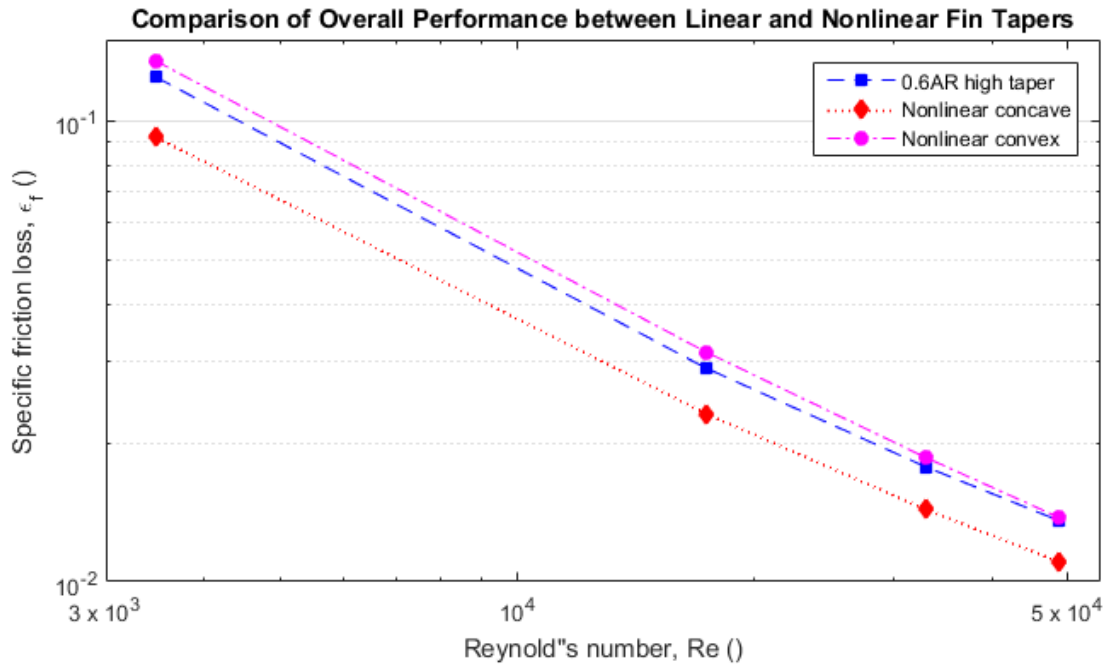


Figure 16: Performance comparison between the 0.6AR array geometry with linear high taper, concave taper, and convex taper, including calculated best fit lines.

Comparison of Double and Triple Repeating Fin Patterns

Figure 13 shows that pin fin arrays with staggered rows repeating every three instances are viable candidate designs for further study on an overall performance basis. These arrays were modelled on the 0.6AR low and high taper arrays, with equivalent streamwise and spanwise fin spacing, but rearranged to form the triple row pattern. This led to a decrease in the total number of pins over the array and subsequently more volume in the inter-fin region, so direct quantitative comparisons require further study. Still, normalized velocity contour plots for the double- and triple-repeating arrays of 0.6AR pin fins are shown in Figure 17, and allow us to quantitatively compare the fluid flow in each configuration.

It is observed that the triple row pattern produces a less linear configuration of fluid flow, with a higher degree of spanwise motion. Impinging flow on the front of each fin is shed to the inter-fin region where, instead of continuing straight through to the outlet, encounters the shoulder of another fin. This cascade effect served to increase both turbulence and heat transfer.

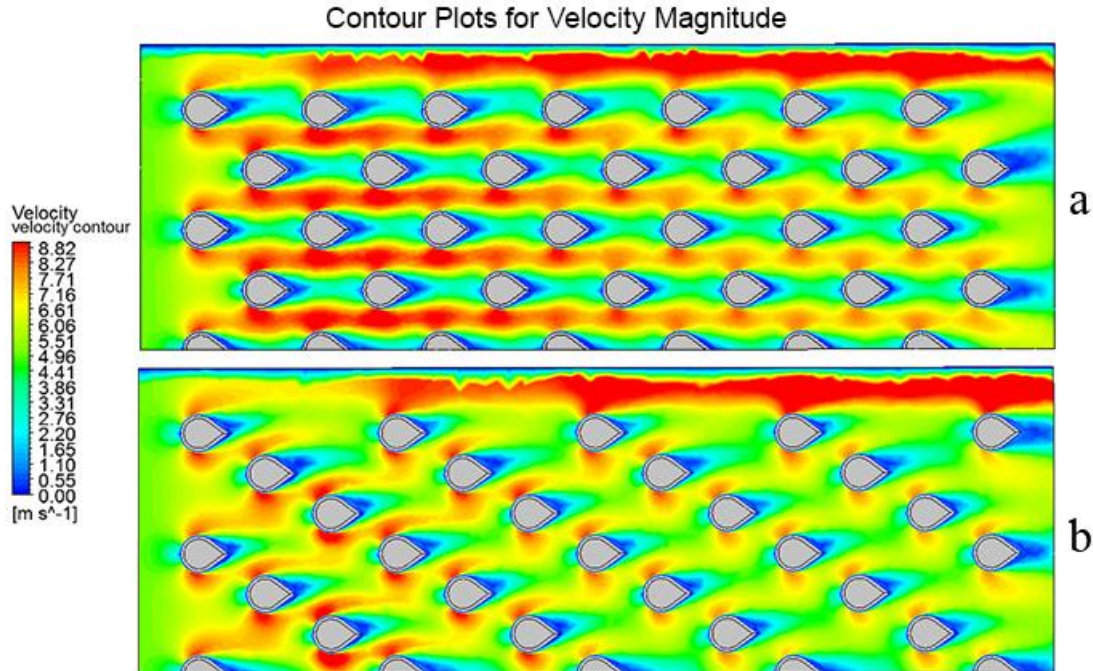


Figure 17: Normalized velocity contour plots of the fluid volume, taken on the horizontal midplane of each fin array. a) 0.6AR low taper, b) (0.6AR) triple row low taper.

Achieving Optimal Performance

The overall highest performing geometry observed in this work is the 0.2AR high taper array (Figure 13). The high aspect ratio teardrop shape effectively reduces turbulence and vortex shedding in the wake of the fin, delays boundary layer separation, and the high taper increases heat transfer performance at the tip of the fin while allowing greater fluid flow. As a result, the overall pressure loss experienced by this fin array was minimized, with respect to the proportional increase in heat transfer efficiency.

The general trends observed by previous work are that increasing aspect ratio of teardrop fins increases their overall performance [11], [13], and increased array density can lead to increased overall performance [5], [9]. In this work it was observed that overall performance can be increased by using high taper angles, nonlinear taper profiles, and variations on the staggered array pattern, as well as reducing fin diameter along the streamwise axis.

Following these trends to their conclusions, using 0.1AR or similar extremely high aspect ratio fins, utilizing a high taper angle with nonlinear concave profile, in a more condensed version of the triple or quadruple row repeating layout pattern, with variable diameter along the length of the array, could achieve more optimal results than those found in this work. Mechanical design considerations would need to be addressed; the fin tail ends may be fragile to debris or highly turbulent flow, and the arrays may become impractically long to maintain proper fin spacing.

Future Work

Diameter Changing Fin Arrays

Future work in this area should include alternative diameter reduction schemes should be investigated, both less and more aggressive than 5% per row. It should also include varying the aspect ratio and taper parameters of fins along the streamwise length, instead of solely the fin diameter. In theory it should be possible to discretize this type of array into quantitative parameters, which could be inserted into a machine learning algorithm to intelligently optimize the shapes, locations, and characteristics of each individual pin for a specific flow regime. The outputs of this algorithm would be used as design parameters for computational testing, similar to the process employed by Wu et al. utilizing genetic algorithms [28].

Nonlinear and Variable Cross-Section Tapered Fins

Future work in optimization should be conducted, defining fin profile based on a theoretical and simulated analysis of steady-state vertical temperature profiles along the length of each fin. Malekzadeh et al. introduced an accurate two-dimensional numerical tool for analysis of nonlinear fins in [27], which could be employed or extended to 3D for use in the design stage. In addition to the taper profile, varying the cross-sectional geometry as a function of fin height should also be investigated. Optimization using both methods could be further accomplished through iterative machine learning or design of experiment testing.

Triple Row Repeating Fin Arrays

The increase in fluid-fin interaction caused by the triply staggered rows is responsible for enhanced heat transfer within the fin array. Future work should be conducted on these triple row repeating arrays, investigating the effects of streamwise and spanwise spacing on tapered pin fins of various cross-sectional geometries.

Teardrop Fin Arrays at High Reynold's Numbers

Future work should be conducted to confirm the relative performance of straight teardrop pin fins at high Reynold's number when compared to tapered analogues. The lack of such a relationship in the SEF geometry family leads this author to believe it may have been an artifact derives of some part of the simulation design.

Summary

To study the effects of novel tapered pin fins shapes and arrangements on heat transfer efficiency, pressure loss, and overall performance, 21 fin arrays were designed and implemented across eight geometry families with varying fin cross-section, taper angle, taper profile, and array patterns.

Experimental testing was carried out on a prototype open-loop wind tunnel system using differential pressure sensors to measure pressure drop across the test section directly, and inlet flow velocity indirectly using a pitot-static tube. The fin arrays were fabricated in Nylon 12 using laser sintering, and data gathered using at $0 < Re < 50,000$.

Computational fluid dynamics simulations were designed in ANSYS to model pressure drop and heat transfer across heated aluminum versions of the same fin arrays. Experimental pressure drop data was used as validation for the simulated fluid flow, and as a confidence metric for the accuracy of the simulated heat transfer.

The experimental and computational data were reduced and analyzed using Matlab, defining non-dimensional metrics for holistic comparison between the disparate array geometries and layouts. These metrics were used to compare heat transfer efficiency, pressure loss characteristics, and overall balanced performance between fin arrays.

Comparisons were made between members of each geometry family, as well as between geometry families, to illuminate effective means for increasing overall heat exchanger performance. Topics for future work and potential methods of investigation were suggested.

Conclusions

1. Teardrop shaped pin fins effectively increase the performance of pin fin arrays by delaying boundary layer separation, and wake field turbulence.
2. High aspect ratio teardrop fins are desired to maximize these effects and attain the greatest overall performance.
3. Tapered pin fins in any cross-sectional geometry are more effective than straight pin fins in equal flow regimes.
4. Of the 21 tested fin arrays, the 0.2AR high taper array was the overall highest performing geometry.
5. Varying fin dimensions along the streamwise axis can effectively increase the performance of drop-shaped pin fin arrays. These configurations should be investigated in more detail.
6. Using nonlinear concave taper profiles can effectively increase the performance of drop-shaped pin fins. This type of fin geometry should be investigated in more detail.
7. Alternative fin placement configurations, such as triple row repeating staggered arrays, can effect more spanwise fluid movement and ultimately increase the performance of drop-shaped pin fin arrays. These configurations should be investigated in more detail.

References

- [1] C. L. Chapman, S. Lee, and B. L. Schmidt, "Thermal Performance of an Elliptical Pin Fin Heat Sink," *Proc. 1994 IEEE/CHMT 10th Semicond. Therm. Meas. Manag. Symp.*, 1994, 1994.
- [2] O. Uzol and C. Camci, "Elliptical Pin Fins As an Alternative To Circular Pin Fins for Gas Turbine Blade Cooling Applications, Part 1," *ASME Turbo Expo 2001 Power Land, Sea, Air*, vol. 3, 2001, 2001.
- [3] G. J. VanFossen, "Heat-Transfer Coefficients for Staggered Arrays of Short Pin Fins," *J. Eng. Power*, vol. 104, no. 2, Apr. 1982, pp. 268–274, Apr. 1982.
- [4] D. E. Metzger, R. A. Berry, and J. P. Bronson, "Developing Heat Transfer in Rectangular Ducts With Staggered Arrays of Short Pin Fins," *J. Heat Transfer*, vol. 104, no. 4, 1982,

- p. 700, 1982.
- [5] N. Sahiti, "Thermal and Fluid Dynamic Performance of Pin Fin Heat Transfer Surfaces," 2006, 2006.
 - [6] A. Armellini, L. Casarsa, and P. Giannattasio, "Low Reynolds number flow in rectangular cooling channels provided with low aspect ratio pin fins," *Int. J. Heat Fluid Flow*, vol. 31, no. 4, 2010, pp. 689–701, 2010.
 - [7] S. A. Lawson, A. A. Thrift, K. A. Thole, and A. Kohli, "Heat transfer from multiple row arrays of low aspect ratio pin fins," *Int. J. Heat Mass Transf.*, vol. 54, no. 17, 2011, pp. 4099–4109, 2011.
 - [8] P. Naphon and A. Sookkasem, "Investigation on heat transfer characteristics of tapered cylinder pin fin heat sinks," *Energy Convers. Manag.*, vol. 48, no. 10, 2007, pp. 2671–2679, 2007.
 - [9] B. G. Wang and H. H. Ji, "An Experimental Investigation of Heat Transfer and Friction Loss in Taper Pin Fin Configurations of Air Cooled Turbine Blades," in *Proceedings of the ASME-JSME Thermal Engineering Joint Conference*, 1987, vol. 4, pp. 127–133.
 - [10] O. Uzol and C. Camci, "Heat transfer, pressure loss and flow field measurements downstream of staggered two-row circular and elliptical pin fin arrays," *J Heat Transf.* 127(5), vol. 127, no. 5, 2005, pp. 458–471, 2005.
 - [11] F. Wang, J. Zhang, and S. Wang, "Investigation on flow and heat transfer characteristics in rectangular channel with drop-shaped pin fins," *Propuls. Power Res.*, vol. 1, no. 1, 2012, pp. 64–70, 2012.
 - [12] M. Wong, I. Owen, C. J. Sutcliffe, and A. Puri, "Convective heat transfer and pressure losses across novel heat sinks fabricated by Selective Laser Melting," *Int. J. Heat Mass Transf.*, vol. 52, no. 1–2, 2009, pp. 281–288, 2009.
 - [13] O. Uzol, "Novel concepts and geometries as alternatives to conventional circular pin fins for gas turbine blade cooling applications," The Pennsylvania State University, 2000.
 - [14] K. L. Kirsch, J. K. Ostanek, and K. a. Thole, "Comparison of Pin Surface Heat Transfer in Arrays of Oblong and Cylindrical Pin Fins," *J. Turbomach.*, vol. 136, no. 4, 2013, p. 041015, 2013.
 - [15] Q. Li, Z. Chen, U. Flechtner, and H. J. Warnecke, "Heat transfer and pressure drop characteristics in rectangular channels with elliptic pin fins," *Int. J. Heat Fluid Flow*, vol. 19, no. 3, 1998, pp. 245–250, 1998.
 - [16] M. K. Chyu, Y. C. Hsing, and V. Natarajan, "Convective Heat Transfer of Cubic Fin Arrays in a Narrow Channel," *J. Turbomach.*, vol. 120, no. 2, Apr. 1998, pp. 362–367, Apr. 1998.
 - [17] T.-M. Jeng and S.-C. Tzeng, "Pressure drop and heat transfer of square pin-fin arrays in in-line and staggered arrangements," *Int. J. Heat Mass Transf.*, vol. 50, no. 11, 2007, pp. 2364–2375, 2007.
 - [18] Z. Chen, Q. Li, D. Meier, and H.-J. Warnecke, "Convective heat transfer and pressure loss in rectangular ducts with drop-shaped pin fins," *Heat Mass Transf.*, vol. 33, 1997, pp. 219–224, 1997.
 - [19] Stratasys Direct Manufacturing, "Nylon 12 PA Laser Sintering Material Specifications." 2015.
 - [20] L. Cattafesta, C. J. Bahr, and J. Mathew, "Fundamentals of Wind-Tunnel Design," *Encycl. Aerosp. Eng.*, no. December, 2010, 2010.
 - [21] R. D. Mehta and P. Bradshaw, "Design Rules for Small Low Speed Wind Tunnels," *The Aeronautical Journal of the Royal Aeronautical Society*. pp. 443–449, 1979.
 - [22] ANSYS Southpointe, "ANSYS Fluent User's Guide 15.0." ANSYS, Inc., Canonsberg,

- PA, 2013.
- [23] B. R. Munson, D. F. Young, and T. H. Okiishi., *Fundamentals of Fluid Mechanics*, 7th ed. Wiley, 2013.
 - [24] B. Moshfegh and R. Nyiredy, “Comparing RANS Models for Flow and Thermal Analysis of Pin Fin Heat Sinks 1,” no. December, 2004, pp. 2–5, 2004.
 - [25] K. T. Cihã, “Pressure Loss through Multiple Rows of Various Short Pin Array Geometries A Survey of Pressure Loss and Heat Transfer through Multiple Rows of Short Pin Arrays,” 2014, 2014.
 - [26] R. J. Goldstein, M. Y. Jabbari, and S. B. Chen, “Convective mass transfer and pressure loss characteristics of staggered short pin-fin arrays,” *Int. J. Heat Mass Transf.*, vol. 37, no. SUPPL. 1, 1994, pp. 149–160, 1994.
 - [27] P. Malekzadeh and H. Rahideh, “Two-dimensional nonlinear transient heat transfer analysis of variable section pin fins,” *Energy Convers. Manag.*, vol. 50, no. 4, 2009, pp. 916–922, 2009.
 - [28] Z. Wu, M. I. Campbell, and B. R. Fernández, “Bond Graph Based Automated Modeling for Computer-Aided Design of Dynamic Systems,” *J. Mech. Des.*, vol. 130, no. 4, Mar. 2008, p. 41102, Mar. 2008.